

# Neighborhood Homophily-Guided Graph Convolutional Network

Shengbo Gong<sup>1</sup>, Jiajun Zhou<sup>1\*</sup>, Chenxuan Xie<sup>1</sup>, Qi Xuan<sup>1</sup>

<sup>1</sup>Zhejiang University of Technology

{jshmhsb, hello.crabboss}@gmail.com, {jjzhou, xuanqi}@zjut.edu.cn

## Abstract

Graph neural networks (GNNs) have achieved remarkable advances in graph-oriented tasks. However, many real-world graphs contain heterophily or low homophily, challenging the homophily assumption of classical GNNs and resulting in low performance. Although many studies have emerged to improve the universality of GNNs, they rarely consider the label reuse and the correlation of their proposed metrics and models. In this paper, we first design a new metric, named Neighborhood Homophily (*NH*), to measure the label complexity or purity in the neighborhood of nodes. Furthermore, we incorporate this metric into the classical graph convolutional network (GCN) architecture and propose Neighborhood Homophily-Guided Graph Convolutional Network (NHGCN). In this framework, nodes are grouped by estimated *NH* values to achieve intra-group weight sharing during message propagation and aggregation. Then the generated node predictions are used to estimate and update new *NH* values. The two processes of metric estimation and model inference are alternately optimized to achieve better node classification. Extensive experiments on both homophilous and heterophilous benchmarks demonstrate that NHGCN achieves state-of-the-art overall performance on semi-supervised node classification for the universality problem.

## 1 Introduction

Graph-structured data can effectively model real-world interactive systems and has received considerable attention recently. For example, a literature database can be topologized as a citation network, where nodes represent papers with additional information such as authors and keywords as node features, and edges represent citation relationships between papers. With the rapid development of deep learning technology on graphs, graph neural networks (GNNs) have been proven to be powerful in many graph-related applications, including node classification, anomaly detection, community

detection, recommendation systems, etc.

GNNs can be divided into two main categories, spectral domain and spatial domain methods [Zhang *et al.*, 2019]. The former is based on spectral graph theory and convolution theorem, represented by GCN-Cheby [Defferrard *et al.*, 2016] and SGC [Wu *et al.*, 2019], while the latter is based on specially designed aggregation functions, represented by graph convolutional network (GCN) [Kipf and Welling, 2017], Sage [Hamilton *et al.*, 2017] and graph attention network (GAT) [Veličković *et al.*, 2018]. These classical GNN methods can learn node representations by feature propagation and aggregation in the node neighborhood and have been proved powerful on graph datasets that conform to homophily assumption, i.e., nodes generally tend to be connected to nodes with the same label. However, many real-world graphs contain heterophily or low homophily, for example, normal users are usually associated with fraudulent accounts in financial fraud networks. This does not follow the homophily assumption of classical GNNs, making them exposed to too much irrelevant information during message propagation and aggregation, eventually leading to poor performance. Such cases are summarized as the universality problem [Chien *et al.*, 2021], which expects to design models that perform well on various graphs, whether homophilous or heterophilous. In other words, universality requires that models be independent of homophily or heterophily assumptions.

**Related Work** In this regard, we review existing studies that focus on the universality problem and summarize them into two broad categories, spectral and spatial domain methods. Most of the related spectral domain methods adhere to the locality assumption for the universality problem. For example, Mixhop [Abu-El-Haija *et al.*, 2019], H2GCN [Zhu *et al.*, 2020] and Snowball [Luan *et al.*, 2019] enrich local information by concatenating multi-order intermediate representations, while FAGCN [Bo *et al.*, 2021] and ACM [Luan *et al.*, 2022] design local filters to better capture local information. *However, these methods lack effective rules to guide message propagation.* Other related methods espouse the intuition that non-local information might be helpful for heterophilous graph analysis [Liu *et al.*, 2021], so they focus on designing deeper GNNs, since stacking more layers means larger receptive field sizes, allowing nodes to access non-local information. However, too many layers of message aggregation can make the features over-smoothing and indistinguish-

\*Jiajun Zhou is the corresponding author.

able [Li *et al.*, 2018; Oono and Suzuki, 2019], eventually leading to model degradation [Zhang *et al.*, 2022]. Inspired by studies such as [He *et al.*, 2016] in other fields, some tricks like initial connection, skip connection, and linear setting are incorporated into the GNN model design to alleviate over-smoothing. For example, spectral methods like GCNII [Chen *et al.*, 2020a], GPRGNN [Chien *et al.*, 2021] and BernNet [He *et al.*, 2021] make use of polynomial approximation as well as several of the above tricks to design their methods, aiming at alleviating feature over-smoothing and achieving suitable receptive field sizes for learning heterophilous graphs. *However, these deep methods do not change the propagation mechanism that works under homophily assumption and may introduce noise* [Wang *et al.*, 2022].

Spatial domain methods do not rely on spectral graph theory and thus allow reasonable adaptations of message aggregation rules. For example, Masked-GCN [Yang *et al.*, 2019] and DMP [Yang *et al.*, 2021] assign attribute-wise weights to neighbor information during aggregation and can be regarded as more fine-grained GAT. Geom-GCN [Pei *et al.*, 2019] adds virtual nodes to aggregate latent space neighbors and structural neighbors respectively. WRGAT [Suresh *et al.*, 2021] allows structurally similar neighbors to be directly connected on the multi-relationship graph, which may make structurally similar neighbors aware of each other. *These methods require computing aggregated weights or new topologies and are thus time-consuming.* In addition, LINKX [Lim *et al.*, 2021] and GloGNN [Li *et al.*, 2022] separately embeds adjacency information and node features with MLPs and then combines them together with subsequent transformation to make the final predictions. *The direct input of the adjacency matrix into the MLP seems to lack interpretation.* On the other hand, label distribution is the direct reason why nodes or graphs are categorized as homophilous or heterophilous, so the label reuse [Wang, 2021] technique can be helpful. GBK [Du *et al.*, 2022] groups neighbors by whether they are of the same class as the target nodes, soft-separating neighborhoods through a gating mechanism. CPGNN [Zhu *et al.*, 2021] and HOG [Wang *et al.*, 2022] reuse the predicted labels to calibrate the training process. *These methods use labels in an implicit way, such as using label propagation that is still based on homophily assumption, or in an explicit way, such as using label transition matrices to fix unconfirmable transition probabilities between two classes of nodes.* More importantly, some of the above methods propose new metrics to measure homophily, but they do not combine the designed metrics and models well, i.e., *these homophily metrics are not well used to guide model learning, which reduces both the rationality of proposed metrics and the theoretical support of proposed models.*

**Contributions** In this paper, we focus on addressing two main drawbacks existing in related methods: 1) Label information is rarely considered or not used properly; 2) The correlation between homophily metrics and models is ignored. We first design a new metric named **Neighborhood Homophily (NH)**, which can measure the label complexity or purity in the receptive fields. Furthermore, we incorporate this metric into classical GCN architec-

ture and propose **Neighborhood Homophily-Guided Graph Convolutional Network (NHGCN)**. In our *NHGCN* framework, nodes are first grouped by estimated *NH* metric, and then different groups of nodes accept adaptive message propagation and aggregation rules to generate their representations and predictions. Subsequently, the generated node predictions are used to estimate and update the *NH* values. During training, the two processes of metric estimation and model inference are alternately optimized to achieve better node classification. Extensive experiments on ten benchmark datasets demonstrate that our proposed framework achieves state-of-the-art performance for the universality problem.

## 2 Preliminaries

An attributed graph can be represented as  $G = (V, E, \mathbf{X}, \mathbf{Y})$ , where  $V$  and  $E$  are the sets of nodes and edges respectively,  $\mathbf{X} \in \mathbb{R}^{|V| \times f}$  is the node feature matrix, and  $\mathbf{Y} \in \mathbb{R}^{|V| \times C}$  is the node label matrix. Here we use  $|V|$ ,  $f$ ,  $C$  to denote the number of nodes, the dimension of the node features, and the number of node classes, respectively. Each row of  $\mathbf{X}$  (i.e.,  $\mathbf{x}_i$ ) represents the feature vector of node  $v_i$ , and each row of  $\mathbf{Y}$  (i.e.,  $\mathbf{y}_i$ ) represents the one-hot label of node  $v_i$ . The structure elements  $(V, E)$  can also be represented as an adjacency matrix  $\mathbf{A} \in \mathbb{R}^{|V| \times |V|}$  that encodes pairwise connections between the nodes, whose entry  $\mathbf{A}_{ij} = 1$  if there exists an edge between  $v_i$  and  $v_j$ , and  $\mathbf{A}_{ij} = 0$  otherwise. Based on the adjacency matrix, we can define the degree distribution of  $G$  as a diagonal degree matrix  $\mathbf{D} \in \mathbb{R}^{|V| \times |V|}$  with entries  $\mathbf{D}_{ii} = \sum_{j=0}^{|V|} \mathbf{A}_{ij} = d_i$  representing the degree value of  $v_i$ .

### 2.1 Graph Convolutional Network (GCN)

The standard Graph Convolutional Network (GCN) with two layers proposed in [Kipf and Welling, 2017] can be formulated as follows:

$$\mathbf{Y} = \text{Softmax}(\text{norm}(\mathbf{A}) \cdot \text{ReLU}(\text{norm}(\mathbf{A})\mathbf{X}\mathbf{W}_0)\mathbf{W}_1) \quad (1)$$

where the output  $\mathbf{Y}$  is the soft assignment of label predictions, and  $\text{norm}(\cdot)$  is the symmetric normalization operation with  $\text{norm}_i(\mathbf{A}) = \mathbf{D}^{-1/2}\mathbf{A}\mathbf{D}^{-1/2}$  or  $\text{norm}(\mathbf{A}) = (\mathbf{D} + \mathbf{I})^{-1/2}(\mathbf{A} + \mathbf{I})(\mathbf{D} + \mathbf{I})^{-1/2}$ . GCN can be trained by minimizing cross-entropy loss on semi-supervised node classification.

### 2.2 Node Homophily

To address the universality problem, a number of metrics have been proposed to measure the node or graph homophily. One of the most widely used metrics is node homophily [Pei *et al.*, 2019], which can be defined as follows:

$$\begin{aligned} \text{node-level: } \mathcal{H}_i^{\text{node}} &= \frac{1}{d_i} \cdot |\{v_j \mid (v_i, v_j) \in E, y_i = y_j\}| \\ \text{graph-level: } \mathcal{H}_G^{\text{node}} &= \frac{1}{|V|} \sum_{v_i \in V} \mathcal{H}_i \end{aligned} \quad (2)$$

where  $y$  represents the node label. Node-level homophily represents the proportion of nodes that have the same label as the target node among its direct neighbors. It is limited to first-order neighborhoods, making it difficult to glimpse more wider heterophily.

### 3 Neighborhood Homophily Metric

#### 3.1 Observation and Definition

Generally, heterophily is not conducive to classical GNNs, because intuitively, the features of different classes of nodes will be inappropriately mixed during message aggregation, resulting in the learned node features being indistinguishable [Zhu *et al.*, 2020]. However, GCN still performs well on bipartite graphs, which are completely heterophilous under the definition of node homophily metric, bringing contradictory judgments [Ma *et al.*, 2021]. As illustrated in Fig. 1, node homophily ( $\mathcal{H}^{node} = 0$ ) cannot explain the fact that GCN can still perform well on bipartite graphs. A new metric called **aggregated similarity score** [Luan *et al.*, 2022] has been proposed to alleviate this contradiction, which can be calculated by the similarity of intermediate representations and label consistency, but has high computational complexity. In this paper, in order to overcome the shortcomings of traditional homophily metrics, we propose a new metric named **Neighborhood Homophily (NH)**, which can measure the label complexity or purity in the neighborhood of target nodes. For a target node  $v_i$ , its  $k$ -hop neighborhood homophily  $NH_i^k$  can be defined as follows:

$$NH_i^k = \frac{|\mathcal{N}(i, k, c_{max})|}{|\mathcal{N}(i, k)|}$$

with  $c_{max} = \arg \max_{c \in [1, C]} |\mathcal{N}(i, k, c)|$  (3)

$$\mathcal{N}(i, k, c) = \{v_j \mid v_j \in \mathcal{N}(i, k), y_j = c\}$$

where  $\mathcal{N}(i, k) = \{v \mid 1 \leq \text{ShortestPath}(v_i, v) \leq k\}$  means the set of neighbors in the  $k$ -hop neighborhood of  $v_i$ ,  $\mathcal{N}(i, k, c)$  means the set of neighbors whose node label is  $c$  in the  $k$ -hop neighborhood of  $v_i$ . Unlike most other homophily metrics,  $NH$  ignores the label information of the target node itself, and only considers the label distribution of other nodes in the  $k$ -hop neighborhood.  $NH = 1$  in Fig. 1 indicates that the neighborhood homophily metric considers the neighborhood of the nodes in the bipartite graph to have the lowest complexity (or the highest purity) and will not confuse GCN.

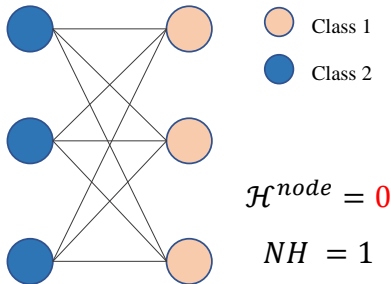


Figure 1: Case shows that neighborhood homophily metric can measure the prediction ability of GNN but node homophily metric fails.

To determine the range of values for  $NH$  metric, we consider the following three extreme cases: 1) Assuming that all neighbors in the neighborhood have the same label, i.e., a completely homophilous neighborhood, then  $NH = 1$ ; 2)

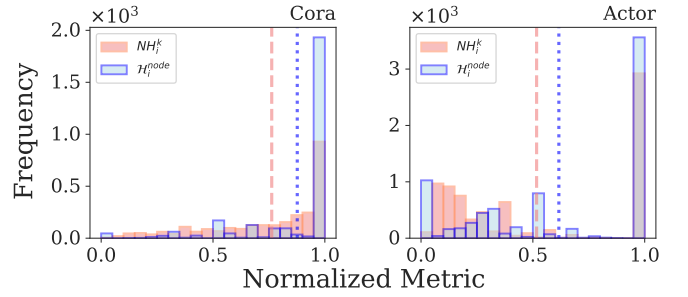


Figure 2: The distribution difference of neighborhood homophily metric and node homophily metric on different datasets. The vertical dashed line represents the mean value.

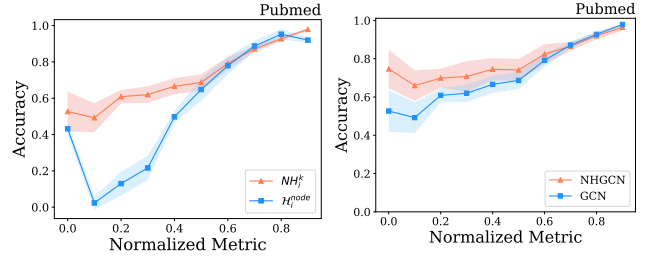


Figure 3: Correlation between node classification accuracy of GCN and different metric groups.

Figure 4: Node classification accuracy of the two models under different  $NH$  metric groups.

Assuming that the neighborhood contains nodes of all label types and the label distribution is balanced, i.e., an extremely complex neighborhood, then  $NH = \frac{1}{C}$ ; 3) For an isolated node, we set the value to 1. In summary, for a graph with  $C$  types of node labels, we have  $NH \in [\frac{1}{C}, 1]$  for an arbitrary node in this graph. Note that in order to better compare the above two metrics, we will perform normalization to unify their value ranges to  $[0, 1]$ .

#### 3.2 Analysis and Comparison

To exhibit the difference between our neighborhood homophily metric and the node homophily metric, we compare their distributions on the homophilous dataset *Cora* and heterophilous dataset *Actor*, as shown in Fig. 2. Here we set  $k = 2$  and calculate the normalized metrics. On *Cora*,  $NH$  metric shows an approximately exponential distribution, while node homophily metric behaves more extremely. On *Actor*, the two metrics show multimodal distribution but have certain differences from each other.

Since classical GNNs such as GCN are designed based on homophily assumptions, they naturally perform poorly in low-homophily scenarios. Therefore, a well-designed homophily metric should behave consistently with the performance of GCN. We use these two metrics to group the nodes (ten groups from 0 to 1 with an interval of 0.1) and then performed the accuracy analysis on the standard GCN<sup>1</sup>, as shown in Fig. 3. The accuracy curve represented by the  $NH$

<sup>1</sup>Standard GCN: 2 layers with 64 hidden units, 0.5 dropout rate, and ReLU.

# Neighborhood Homophily-Guided Graph Convolutional Network

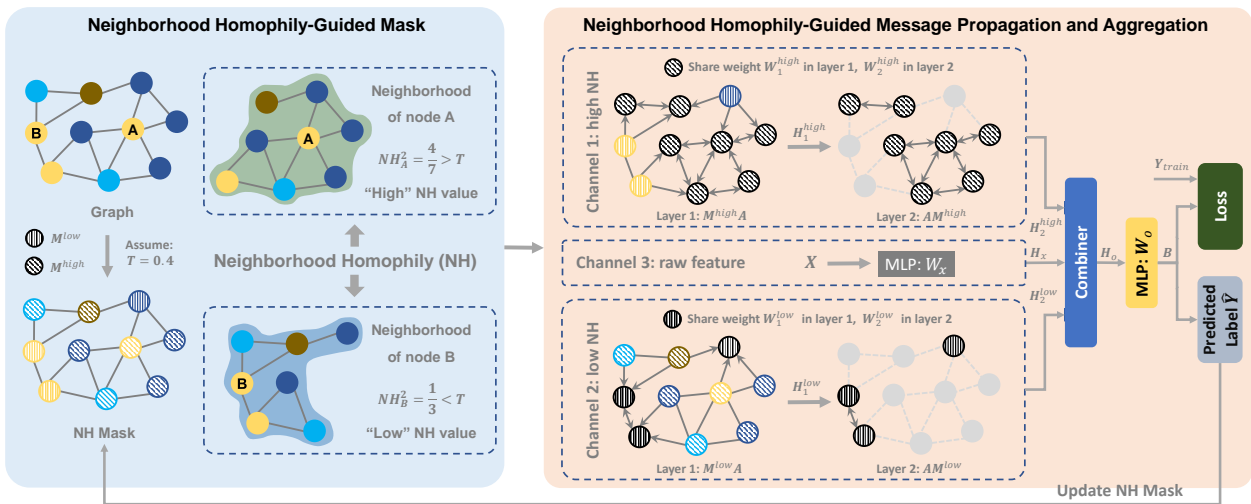


Figure 5: Schematic depiction of *NHGCN* framework. The complete workflow proceeds as follows: (1) Calculate the *NH* values of nodes and generate the *NH* masks, which can divide all nodes into two groups (high *NH* and low *NH*); (2) The two groups of nodes are asymmetrically aggregated in two different channels, the raw features of the nodes are mapped in the third channel, and the outputs of the three channels are combined for subsequent model prediction; (3) The predicted labels are used to update the *NH* values of all nodes, and then the above two processes are repeated until the model converges.

metric rises almost monotonically, which well reflects that with higher neighborhood homophily, GCN performs better for prediction. However, the GCN model has abnormally high prediction accuracy for the nodes with the lowest node homophily. The above phenomenon well illustrates that *NH* metric can better measure the difficulty of classifying nodes for GCN, i.e., *NH* is a better metric than node homophily. Meanwhile, we also compare the prediction results of the proposed model and the GCN model for different groups of nodes, as shown in Fig. 4, from which we can see that with the guidance of *NH* metric, our proposed model can better predict low-homophily nodes while maintaining the prediction effect on high-homophily nodes when compared with GCN.

## 4 Methodology

### 4.1 Motivations

Based on the above observations and analysis, we find that *NH* metric can estimate the homophily by measuring the complexity of the neighborhood labels, which is more robust and capable than other metrics that consider target nodes. Intuitively, nodes with highly homophilous neighborhoods generally behave differently than nodes with highly heterophilous neighborhoods. For example, some authors will have a preference for citing papers from multiple fields, while others limit themselves to their own fields [Bornmann and Daniel, 2008]. It is not expected to share the same learner or message propagation rule between “outward” and “inward” nodes. Therefore, we propose a novel approach — Neighborhood Homophily-Guided Graph Convolutional Network (*NHGCN*), in which nodes are grouped by neighborhood homophily metric, and nodes in different groups accept different message propagation and aggregation rules. Fig. 5 outlines the overall framework of our method.

### 4.2 Neighborhood Homophily-Guided Mask

As demonstrated above, *NH* metric can effectively measure the complexity of node neighborhoods. So we incorporate it into the GCN model to guide message propagation, by distinguishing nodes into high and low homophily nodes. According to Eq. (3), the calculation of *NH* metric relies on node label information, but it is illegal to use labels other than the training set during the training process. So we use the predicted labels to calculate the *NH* metric. Specifically, we first initialize the *NH* values of all nodes to 1, and then update the *NH* values at each subsequent time when the update condition is met according to Eq. (3) and the predicted labels:

$$NH_i^k(t+1) = \frac{|\mathcal{N}(i, k, c_{max})|}{|\mathcal{N}(i, k)|} \quad (4)$$

with  $c_{max} = \arg \max_{c \in [1, C]} |\mathcal{N}(i, k, c)|$

$$\mathcal{N}(i, k, c) = \{v_j \mid v_j \in \mathcal{N}(i, k), \hat{y}_j(t) = c\}$$

where  $\hat{y}_j(t)$  represents the predicted label of node  $v_j$  in  $t$ -th update (see Sec. 4.4). After updating the *NH* value of each node, we utilize a threshold  $T$  to distinguish the nodes into high and low homophily nodes, from which we can get the Neighborhood Homophily-Guided Masks (*NH* mask):

$$\begin{aligned} M_{ii}^{low}(t) &= \mathbb{I}(NH_i^k(t) \leq T) \\ M^{high}(t) &= I - M^{low}(t) \end{aligned} \quad (5)$$

where  $\mathbb{I}(\cdot)$  is the indicator function. Nodes with *NH* values above (or below) the threshold are treated as having neighborhoods with high (or low) homophily. Note that both  $M^{low}(t)$  and  $M^{high}(t)$  are diagonal matrices. Although this is not an elegant way due to the introduction of threshold hyper-parameters, the absolute separation of nodes by setting threshold ensures the hard topology optimization, similar to [Chen *et al.*, 2020b; Klicpera *et al.*, 2019].

### 4.3 Neighborhood Homophily-Guided Message Propagation and Aggregation

As mentioned above, nodes with different neighborhood homophily have different behavior patterns, and we want to adopt adaptive message propagation and aggregation for different nodes during training and inference. Here we propose the Neighborhood Homophily-Guided Message Propagation and Aggregation, which utilizes the  $NH$  masks generated in Sec. 4.2 to guide the message propagation and aggregation in the neighborhood of different nodes, as defined below:

$$\begin{aligned} \text{Layer 1: } \mathbf{H}_1^s &= \sigma(\text{norm}(\mathbf{M}^s \mathbf{A}) \cdot \mathbf{X} \mathbf{W}_1^s) \\ \text{Layer 2: } \mathbf{H}_2^s &= \sigma(\text{norm}(\mathbf{A} \mathbf{M}^s) \cdot \mathbf{H}_1^s \mathbf{W}_2^s) \end{aligned} \quad (6)$$

where  $s \in \{low, high\}$  represents different learning channels,  $\mathbf{W}_1^s \in \mathbb{R}^{f \times f'}$ ,  $\mathbf{W}_2^s \in \mathbb{R}^{f' \times f'}$  are the weight matrices,  $\sigma(\cdot)$  is the activation function,  $f'$  denotes the dimension of hidden layers. In the first layer, the left multiplication by  $\mathbf{M}^s$  implies performing row masking or *target masking* on  $\mathbf{A}$ , which can make the adjacency matrix retain only the adjacency information (rows) of high or low homophily nodes (targets), and further realize the weight separation of these two groups of nodes, i.e., the weight  $\mathbf{W}_1$  is not shared between high and low homophily nodes. In doing so, the  $\mathbf{H}_1$  will only aggregate all the first-order information for one group of nodes (high or low homophily) and keep all zero in the masked rows. In the second layer, the right multiplication by  $\mathbf{M}^s$  implies performing column masking or *source masking* on  $\mathbf{A}$ , which can filter out the noisy information (nodes of different groups from the target node) in the neighborhood of the target node (determined in the first layer), so that the target node will only aggregate the information of the same group of neighbors (sources) in the neighborhood:

$$\text{target} \leftarrow \text{source} \in \{low \leftarrow low, high \leftarrow high\} \quad (7)$$

The above two channels  $s \in \{low, high\}$  are used to characterize nodes with high and low neighborhood homophily, respectively. However, for those isolated nodes that have no neighborhood, we cannot effectively measure them with the  $NH$  metric. Therefore, we introduce a third channel to preserve the raw features of nodes:

$$\mathbf{H}_x = \mathbf{X} \mathbf{W}_x \quad (8)$$

where  $\mathbf{W}_x \in \mathbb{R}^{f \times f'}$ . Notice that only linear transformation are applied here for computational efficiency. Finally, we combine the representations from the three channels and derive the soft assignment prediction  $\mathbf{B} \in \mathbb{R}^{n \times C}$  through a MLP as follows:

$$\begin{aligned} \mathbf{H}_o &= \text{combine}(\mathbf{H}_2^{low}, \mathbf{H}_2^{high}, \mathbf{H}_x) \\ \mathbf{B} &= \text{softmax}(\mathbf{H}_o \mathbf{W}_o) \end{aligned} \quad (9)$$

where  $\mathbf{W}_o \in \mathbb{R}^{f \times C}$  is the weight matrix in the MLP,  $\text{combine}(\cdot)$  represents a channel combination operation selected from  $\{add, concatenate, maxpooling\}$ . For the first two combiners, softmax-constrained weights ( $\alpha_{high}, \alpha_{low}, \alpha_x$ , refer to Fig. 7) are used, which means that  $\mathbf{H}_o$  is a convex combination of the output of these three channels:

$$\begin{aligned} \text{add: } \mathbf{H}_o &= \alpha_{low} \mathbf{H}_2^{low} + \alpha_{high} \mathbf{H}_2^{high} + \alpha_x \mathbf{H}_x \\ \text{concatenate: } \mathbf{H}_o &= \alpha_{low} \mathbf{H}_2^{low} \oplus \alpha_{high} \mathbf{H}_2^{high} \oplus \alpha_x \mathbf{H}_x \end{aligned} \quad (10)$$

where  $\oplus$  is the concatenation operation and  $\alpha_{low} + \alpha_{high} + \alpha_x = 1$ . For *maxpooling*, there is no such weight.

### 4.4 Model Training

We employ the cross-entropy as the loss:

$$\mathcal{L} = -\text{trace}(\mathbf{Y}_{train}^\top \log \mathbf{B}) \quad (11)$$

where  $\text{trace}(\cdot)$  means the sum of the diagonal elements of the matrix. The training process is shown in Algorithm 1. During training, once the validation accuracy reaches a new high, the  $NH$  values and masks of all nodes will be recalculated and updated and applied to the subsequent epoch (line 6 and 11).

### 4.5 Variants

The first layer defined in Eq. (6) can be changed to:

$$\mathbf{H}_1^s = \sigma(\text{norm}(\mathbf{A} \mathbf{M}^s) \cdot \mathbf{X} \mathbf{W}_1^s) \quad (12)$$

which implies that the model performs two layers of neighborhood filtering with the same *source mask* and keeps weight sharing between the two channels (*low* and *high*).

---

#### Algorithm 1 Training NHGCN

---

**Require:** Graph  $G = (V, E, \mathbf{X}, \mathbf{Y})$ , hop  $k$ , threshold  $T$ , maximum epochs  $E$ , early stopping patience  $S$ .

**Ensure:** Testing accuracy  $Acc_{test}$ .

- 1: Initialize best validation accuracy:  $Acc_{max} \leftarrow 0$ ;
  - 2: Initialize  $NH$  value for  $\forall v_i \in V$ :  $NH_i^k \leftarrow 1$ ;
  - 3: **for**  $e = 1$  to  $E$  **do**
  - 4:   Get  $NH$  mask via Eq. (5);
  - 5:   Train  $NHGCN$  via Eq. (6) - (11);
  - 6:   Get predicted labels  $\hat{Y}$ , validation accuracy  $Acc_{val}$ ;
  - 7:   **if**  $Acc_{val} > Acc_{max}$  **then**
  - 8:      $Acc_{max} \leftarrow Acc_{val}$ ;
  - 9:     Update  $NH_i^k$  for  $\forall v_i \in V$  by Eq. (4);
  - 10:   **end if**
  - 11:   **if**  $Acc_{val} \leq Acc_{max}$  for  $S$  epochs **then**
  - 12:     Break;
  - 13:   **end if**
  - 14: **end for**
  - 15: Calculate testing accuracy  $Acc_{test}$ ;
  - 16: **return**  $Acc_{test}$ .
- 

## 5 Evaluations

### 5.1 Datasets

We use 10 real-world benchmark datasets as in [Chien *et al.*, 2021], among which the first five (*Cora*, *Citeseer*, *Pubmed*, *Amazon Computer* and *Photo*) are homophilous datasets and the last five (*Chameleon*, *Squirrel*, *Actor*, *Texas* and *Cornell*) are heterophilous datasets. For all datasets, we adopt dense data splitting as in [Chien *et al.*, 2021], i.e., each dataset is randomly split into training / validation / testing samples with a proportion of 60% / 20% / 20%. Under the rule of semi-supervised learning, we can utilize the feature information of all nodes ( $\mathbf{X}$ ) as well as the label information of the training set ( $\mathbf{Y}_{train}$ ) during the training process. Please refer to Appendix A for more data details.

Table 1: Results on real-world benchmark datasets: Mean Test Accuracy (%)  $\pm$  Standard Deviation (%). Boldface letters are used to mark the best results while underlined letters indicate the second best.

	Cora	Citeseer	Pubmed	Computers	Photo		Chameleon	Actor	Squirrel	Texas	Cornell	
#Nodes	2708	3327	19717	13752	7650		2277	7600	5201	183	183	
#Edges	5278	4552	44324	245861	119081		31371	26659	198353	279	277	
$\mathcal{H}^{node}$	0.656	0.578	0.644	0.272	0.459		0.024	0.008	0.055	0.016	0.137	
$NH^1$	0.901	0.904	0.933	0.848	0.882		0.540	0.762	0.455	0.714	0.773	
$NH^2$	0.815	0.834	0.821	0.665	0.727		0.357	0.613	0.291	0.651	0.538	
MLP	73.74 $\pm$ 1.73	76.85 $\pm$ 1.11	84.92 $\pm$ 0.51	57.60 $\pm$ 0.74	38.84 $\pm$ 0.88	11.6	47.11 $\pm$ 4.03	36.33 $\pm$ 0.88	22.56 $\pm$ 3.87	80.98 $\pm$ 7.01	82.34 $\pm$ 5.12	10.8
GCN	87.50 $\pm$ 1.56	81.11 $\pm$ 1.06	89.36 $\pm$ 0.27	90.04 $\pm$ 0.48	94.59 $\pm$ 0.44	7.6	67.83 $\pm$ 2.74	34.94 $\pm$ 1.20	54.01 $\pm$ 1.52	79.18 $\pm$ 3.94	88.24 $\pm$ 1.50	7.6
GCNII	88.65 $\pm$ 0.86	81.04 $\pm$ 0.98	91.37 $\pm$ 0.55	90.63 $\pm$ 0.54	<u>95.55 <math>\pm</math> 0.26</u>	4.4	64.42 $\pm$ 3.07	42.85 $\pm$ 1.04	50.47 $\pm$ 1.61	89.34 $\pm$ 4.18	84.47 $\pm$ 4.82	6.2
BernNet	<u>89.31 <math>\pm</math> 0.75</u>	81.80 $\pm$ 1.50	91.04 $\pm$ 0.32	90.64 $\pm$ 0.61	95.40 $\pm$ 0.44	4.4	69.08 $\pm$ 1.57	42.13 $\pm$ 1.04	<u>58.37 <math>\pm</math> 1.80</u>	91.15 $\pm$ 2.21	90.00 $\pm$ 2.25	3.4
GPRGNN	<b>89.46 <math>\pm</math> 1.40</b>	81.84 $\pm$ 1.08	91.07 $\pm$ 0.69	90.55 $\pm$ 0.39	<b>95.58 <math>\pm</math> 0.46</b>	<u>3.0</u>	68.34 $\pm$ 1.05	42.53 $\pm$ 1.10	53.20 $\pm$ 1.62	90.66 $\pm$ 4.58	88.72 $\pm$ 6.50	4.6
ACM-GCN	87.80 $\pm$ 1.23	<u>82.05 <math>\pm</math> 1.26</u>	90.59 $\pm$ 0.44	90.62 $\pm$ 0.29	95.46 $\pm$ 0.28	4.8	<u>69.79 <math>\pm</math> 3.45</u>	39.78 $\pm$ 1.40	<b>60.43 <math>\pm</math> 1.23</b>	91.48 $\pm$ 2.29	88.09 $\pm$ 3.20	4.2
FAGCN	88.90 $\pm$ 0.88	80.78 $\pm$ 0.95	89.37 $\pm$ 0.48	84.82 $\pm$ 1.52	93.71 $\pm$ 0.96	7.4	60.22 $\pm$ 3.26	41.53 $\pm$ 0.70	42.49 $\pm$ 1.47	88.52 $\pm$ 4.95	89.57 $\pm$ 3.94	7.0
GBK	88.69 $\pm$ 0.42	79.18 $\pm$ 0.96	89.11 $\pm$ 0.23	58.85 $\pm$ 1.32	57.17 $\pm$ 4.86	9.2	48.56 $\pm$ 3.03	38.97 $\pm$ 0.97	31.91 $\pm$ 1.01	81.08 $\pm$ 4.88	74.27 $\pm$ 2.18	10.2
HOG	82.48 $\pm$ 2.94	78.96 $\pm$ 1.52	OOM	64.57 $\pm$ 2.05	71.57 $\pm$ 3.39	10.6	49.87 $\pm$ 2.77	40.65 $\pm$ 1.10	31.66 $\pm$ 1.31	77.05 $\pm$ 5.13	74.89 $\pm$ 6.71	10.2
WRGAT	88.20 $\pm$ 2.26	76.81 $\pm$ 1.89	88.52 $\pm$ 0.92	88.72 $\pm$ 0.84	94.45 $\pm$ 0.49	9.2	65.24 $\pm$ 0.87	36.53 $\pm$ 0.77	48.85 $\pm$ 0.78	83.62 $\pm$ 5.50	81.62 $\pm$ 3.90	8.6
NHGCN	89.05 $\pm$ 1.00	81.95 $\pm$ 0.85	<u>91.58 <math>\pm</math> 0.54</u>	<b>90.73 <math>\pm</math> 0.55</b>	95.24 $\pm$ 0.52	<b>2.8</b>	<b>69.85 <math>\pm</math> 1.14</b>	<u>42.86 <math>\pm</math> 1.25</u>	51.02 $\pm$ 1.25	<u>93.61 <math>\pm</math> 3.32</u>	<u>90.64 <math>\pm</math> 4.51</u>	<b>2.4</b>
NHGCN-SS	88.72 $\pm$ 1.61	<b>82.18 <math>\pm</math> 0.97</b>	<b>91.64 <math>\pm</math> 0.40</b>	90.72 $\pm$ 0.64	95.23 $\pm$ 0.41	3.0	68.99 $\pm$ 1.63	<b>42.94 <math>\pm</math> 0.99</b>	49.99 $\pm$ 1.74	<b>93.93 <math>\pm</math> 2.19</b>	<b>91.28 <math>\pm</math> 4.07</b>	2.8

## 5.2 Comparison Methods

We compare *NHGCN* and its variants with three categories of ten baselines, including two-layer MLP and GCN [Kipf and Welling, 2017] for basic methods, GCNII [Chen *et al.*, 2020a], BernNet [He *et al.*, 2021], GPRGNN [Chien *et al.*, 2021], ACM-GCN [Luan *et al.*, 2022] and FAGCN [Bo *et al.*, 2021] for spectral methods, GBK [Du *et al.*, 2022], HOG [Wang *et al.*, 2022] and WRGAT [Suresh *et al.*, 2021] for spatial methods. Refer to Appendix B for more details.

## 5.3 Experiment Setup

Considering the sensitivity of the results to random seeds, we set ten seeds to fix the data splitting and model initialization. Since most baselines neglect this issue, we utilize their open-source code to reproduce their results under our multiple random seed setting. Finally, we run all experiments ten times with ten random seeds and report the average test accuracy as well as the standard deviation of all methods under different data sets. We also compare our results with those provided in the original paper of baselines in the Appendix D. For all methods, we use the Adam optimizer [Kingma and Ba, 2014] and set the maximum epochs to 500 with 100 epochs patience for early stopping. The hyper-parameters of our method include the number of hidden units chosen from {64, 128, 256, 512}, learning rate chosen from {0.001, 0.002, 0.005, 0.008, 0.01, 0.02, 0.05, 0.08, 0.1}, weight decay from {0, 5e-5, 1e-4, 5e-4, 1e-3, 5e-3} and dropout chosen from [0, 0.9] with 0.1 intervals. The search space for these common parameters will be shared among all baselines. We have specific hyper-parameters including  $k$  chosen from {1, 2, 3},  $T$  chosen from [1/ $C$ , 1] and combinator chosen from {*add*, *concatenate*, *maxpooling*}. Please refer to Appendix C for more parameter details.

## 5.4 Performance Analysis

We evaluate our *NHGCN* on ten benchmark datasets and the results are reported in Table 1. From top to bottom, we show the results of the three types of baselines (basic, spectral domain, spatial domain), from which we can observe and conclude: 1) Spectral domain baselines have high performance

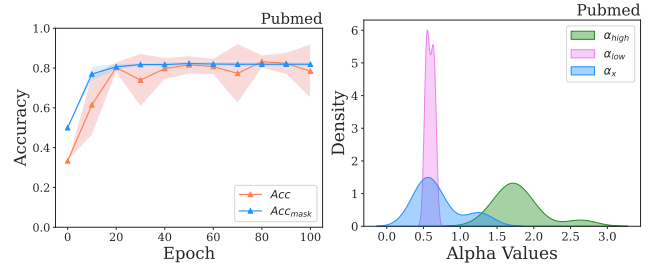


Figure 6: Accuracy curves for metric analysis, where the red and blue curves reflect the change trend of node classification accuracy and mask accuracy, respectively.

Figure 7: The density distribution of the softmax-constrained weights during the channel combination using concatenation.

ranking, especially GPRGNN, which achieves SOTA performance on 2 out of 10 datasets. However, spectral domain methods have different preferences for different datasets. For example, GPRGNN performs better on datasets with high homophily, while BernNet performs better on datasets with high heterophily, which is consistent with the observation in [He *et al.*, 2021]; 2) Spatial domain baselines have a lower performance ranking overall, while performing relatively better on datasets with high heterophily; 3) Compared with ten baselines, our *NHGCN* and its variant achieve the SOTA overall performance and show top two average ranking on both homophilous and heterophilous benchmarks, indicating that our methods are effective and have better universality for different datasets. More specifically, our methods beat strong baselines on 7 out of 10 benchmarks, with relatively higher accuracy and lower variance, guaranteeing the effectiveness and stability; 4) For not achieving good performance on *Squirrel* dataset, we speculate that nodes in *Squirrel* need to be grouped in a more fine-grained way in our frameworks.

## 5.5 Metric Analysis

Our *NHGCN* groups nodes based on the *NH* mask, so its performance depends on the *NH* metric. To further investigate the effectiveness of the *NH* metric, we explored the

correlation between classification accuracy and masking accuracy. We use the ground truth label of all nodes to calculate the real masks (i.e., *real labels*  $\rightarrow$  *real NH values*  $\rightarrow$  *real NH masks*), use the predicted labels of all nodes to estimate the predicted masks (i.e., *predicted labels*  $\rightarrow$  *estimated NH values*  $\rightarrow$  *predicted NH masks*), and finally calculate the masking accuracy through the real masks and the predicted masks. Taking the *Pubmed* dataset as an example, we train our *NHGCN* model under the optimal hyperparameter settings and observe the classification accuracy and masking accuracy under 100 epochs, as shown in Fig. 6. Note that the initial accuracy is set by random guessing. We can observe that with the increase of training epochs, the classification accuracy and masking accuracy show a consistent trend, i.e., they first rise and then tend to be stable. Actually, both classification accuracy and mask accuracy are affected by the estimated *NH* values. During the training process, the model estimates and updates the *NH* values to help itself make better node grouping (masking) and prediction, and a more accurate prediction can in turn promote the estimation of *NH* values. The two processes of metric estimation and model inference are alternately optimized to achieve the convergence of the model, indicating that our *NH* metric and *NHGCN* framework can effectively guide GCN for adaptive message propagation and aggregation. The above phenomenon can also be observed on other datasets.

## 5.6 Ablation Analysis

In our approach, *NH* masks are used to group nodes based on neighborhood homophily. When such grouping strategy is removed, *NHGCN* degenerates to a combination of GCN output and raw features, named *GCN+X* for short. To investigate the effectiveness of this grouping strategy, we compare *NHGCN* and its variant with *GCN+X*, where all nodes are divided into the same group and share the same message propagation and aggregation rule. Results reported in Table 2 show that our methods outperform *GCN+X* on all datasets, verifying the effectiveness of the grouping strategy. In other words, tweaking propagation and aggregation rules for just a few nodes can bring the classification accuracy that meets the bottleneck to new heights. Fig. 7 illustrates that higher weights are assigned to high *NH* group. The contribution of low *NH* group is close to the raw features.

Table 2: Ablation results on real-world benchmark datasets.

	Cora	Citeseer	Pubmed	Computers	Photo
NHGCN	<b>89.05</b> $\pm$ <b>1.00</b>	81.95 $\pm$ 0.85	91.58 $\pm$ 0.54	<b>90.73</b> $\pm$ <b>0.55</b>	<b>95.24</b> $\pm$ <b>0.52</b>
NHGCN-SS	88.72 $\pm$ 1.61	<b>82.18</b> $\pm$ <b>0.97</b>	<b>91.64</b> $\pm$ <b>0.40</b>	90.72 $\pm$ 0.64	95.23 $\pm$ 0.41
GCN+X	88.62 $\pm$ 1.70	81.31 $\pm$ 1.10	90.09 $\pm$ 0.92	89.21 $\pm$ 0.77	94.67 $\pm$ 0.33
	Chameleon	Actor	Squirrel	Texas	Cornell
NHGCN	<b>69.85</b> $\pm$ <b>1.14</b>	42.86 $\pm$ 1.25	<b>51.02</b> $\pm$ <b>1.25</b>	93.61 $\pm$ 3.32	90.64 $\pm$ 4.51
NHGCN-SS	68.99 $\pm$ 1.63	<b>42.94</b> $\pm$ <b>0.99</b>	49.99 $\pm$ 1.74	<b>93.93</b> $\pm$ <b>2.19</b>	<b>91.28</b> $\pm$ <b>4.07</b>
GCN+X	65.67 $\pm$ 2.22	41.83 $\pm$ 1.77	47.23 $\pm$ 1.52	92.46 $\pm$ 1.92	89.36 $\pm$ 4.60

## 5.7 Efficiency Analysis

Since *NHGCN* utilizes GCN-like matrix computation, this part has the same complexity as GCN. We add additional parameters as follows: three adaptive weights, a mask vector, an additional channel, a raw feature channel, and a combiner.

The total number of learnable parameters is  $3 + 2(2(f \times f' + f' \times f')) + f \times f' + 3f' \times c$  flops. If the **maxpooling** combiner is applied, the number of parameters is then subtracted by 3. In addition, for the iterative updates of *NH* mask, we adopt a hash dictionary to quickly index the *k*-hop neighbors of a node. Finally, we follow the scheme of hard topology optimization, which keeps the low memory consumption that comes with sparsity. We also compare *NHGCN* with baselines on actual time consumption, as shown in Table 3. We can observe that the spectral domain methods have better computational efficiency than the spatial domain methods in terms of running time. Since most of the spatial domain methods require additional computational steps to adjust the aggregation rules, mainly through preprocessing, auxiliary tasks, or gating mechanisms. Theoretically, *NHGCN* should have similar execution efficiency to ACM-GCN since both compute three channels in parallel. However, *NHGCN* requires the *bincount* function when updating the *NH* value, which is CPU dependent in engineering, so almost half of the running time is wasted in converting between GPU and CPU cores. Actually, the computational complexity of *NHGCN* is acceptable.

Table 3: Efficiency on *Pubmed* dataset: Average running time per epoch (ms) / average running time in total (s).

	Pubmed
MLP	4.70ms / 1.61s
GCN	7.08ms / 2.06s
GCNII	9.31ms / 3.01s
BernNet	58.52ms / 14.95s
GPRGNN	12.68ms / 3.70s
ACM-GCN	10.76ms / 3.27s
FAGCN	15.40ms / 5.27s
GBK	13346.76ms / 3064.42s
HOG	OOM
WRGAT	1691.71ms / 598.70s
NHGCN	81.45ms / 16.95s
NHGCN-SS	79.42ms / 17.31s

## 6 Conclusions

In this paper, we address two common problems with the universality of existing GNNs: 1) Label reuse is rarely considered or labels are not used properly; 2) The model training process is not associated with the proposed metrics. We design neighborhood homophily as a robust and easy-to-compute metric measuring the homophily. Then we incorporate the proposed metric into classical GCN architecture and propose a neighborhood homophily-guided graph convolutional network (*NHGCN*). Extensive experiments on real-world benchmarks indicate the state-of-the-art overall performance of *NHGCN* for the universality problem.

## Acknowledgments

This work was supported in part by the Key R&D Program of Zhejiang under Grant 2022C01018, by the National Natural Science Foundation of China under Grants 61973273 and

U21B2001, and by the National Key R&D Program of China under Grant 2020YFB1006104.

## References

- [Abu-El-Haija *et al.*, 2019] Sami Abu-El-Haija, Bryan Perozzi, Amol Kapoor, Nazanin Alipourfard, Kristina Lerman, Hrayr Harutyunyan, Greg Ver Steeg, and Aram Galstyan. Mixhop: Higher-order graph convolutional architectures via sparsified neighborhood mixing. In *ICLR*, pages 21–29, 2019.
- [Bergstra *et al.*, 2011] James Bergstra, Rémi Bardenet, Yoshua Bengio, and Balázs Kégl. Algorithms for hyper-parameter optimization. In *NIPS*, volume 24, 2011.
- [Bo *et al.*, 2021] Deyu Bo, Xiao Wang, Chuan Shi, and Huawei Shen. Beyond low-frequency information in graph convolutional networks. In *AAAI*, volume 35, pages 3950–3957, 2021.
- [Bornmann and Daniel, 2008] Lutz Bornmann and Hans-Dieter Daniel. What do citation counts measure? a review of studies on citing behavior. *Journal of documentation*, 2008.
- [Chen *et al.*, 2020a] Ming Chen, Zhewei Wei, Zengfeng Huang, Bolin Ding, and Yaliang Li. Simple and deep graph convolutional networks. In *ICLR*, pages 1725–1735. PMLR, 2020.
- [Chen *et al.*, 2020b] Yu Chen, Lingfei Wu, and Mohammed Zaki. Iterative deep graph learning for graph neural networks: Better and robust node embeddings. In *NIPS*, volume 33, pages 19314–19326, 2020.
- [Chien *et al.*, 2021] Eli Chien, Jianhao Peng, Pan Li, and Olga Milenkovic. Adaptive universal generalized pagerank graph neural network. In *ICLR*, 2021.
- [Defferrard *et al.*, 2016] Michaël Defferrard, Xavier Bresson, and Pierre Vandergheynst. Convolutional neural networks on graphs with fast localized spectral filtering. In *NIPS*, 2016.
- [Du *et al.*, 2022] Lun Du, Xiaozhou Shi, Qiang Fu, Xiaojun Ma, Hengyu Liu, Shi Han, and Dongmei Zhang. Gbk-gnn: Gated bi-kernel graph neural networks for modeling both homophily and heterophily. In *WWW*, pages 1550–1558, 2022.
- [Hamilton *et al.*, 2017] Will Hamilton, Zhitao Ying, and Jure Leskovec. Inductive representation learning on large graphs. volume 30, 2017.
- [He *et al.*, 2016] Kaiming He, Xiangyu Zhang, Shaoqing Ren, and Jian Sun. Deep residual learning for image recognition. In *CVPR*, pages 770–778, 2016.
- [He *et al.*, 2021] Mingguo He, Zhewei Wei, Hongteng Xu, et al. Bernnet: Learning arbitrary graph spectral filters via bernstein approximation. In *NIPS*, volume 34, pages 14239–14251, 2021.
- [Kingma and Ba, 2014] Diederik P Kingma and Jimmy Ba. Adam: A method for stochastic optimization. *arXiv preprint arXiv:1412.6980*, 2014.
- [Kipf and Welling, 2017] Thomas N Kipf and Max Welling. Semi-supervised classification with graph convolutional networks. In *ICLR*, 2017.
- [Klicpera *et al.*, 2019] Johannes Klicpera, Stefan Weissenberger, and Stephan Günnemann. Diffusion improves graph learning. In *NIPS*, pages 13366–13378, 2019.
- [Li *et al.*, 2018] Qimai Li, Zhichao Han, and Xiao-Ming Wu. Deeper insights into graph convolutional networks for semi-supervised learning. In *AAAI*, 2018.
- [Li *et al.*, 2022] Xiang Li, Renyu Zhu, Yao Cheng, Caihua Shan, Siqiang Luo, Dongsheng Li, and Weining Qian. Finding global homophily in graph neural networks when meeting heterophily. In *ICML*, 2022.
- [Lim *et al.*, 2021] Derek Lim, Felix Hohne, Xiuyu Li, Sijia Linda Huang, Vaishnavi Gupta, Omkar Bhalerao, and Ser Nam Lim. Large scale learning on non-homophilous graphs: New benchmarks and strong simple methods. In *NIPS*, volume 34, pages 20887–20902, 2021.
- [Liu *et al.*, 2021] Meng Liu, Zhengyang Wang, and Shuiwang Ji. Non-local graph neural networks. *IEEE Transactions on Pattern Analysis and Machine Intelligence*, 2021.
- [Luan *et al.*, 2019] Sitao Luan, Mingde Zhao, Xiao-Wen Chang, and Doina Precup. Break the ceiling: Stronger multi-scale deep graph convolutional networks. In *NIPS*, volume 32, 2019.
- [Luan *et al.*, 2022] Sitao Luan, Chenqing Hua, Qincheng Lu, Jiaqi Zhu, Mingde Zhao, Shuyuan Zhang, Xiao-Wen Chang, and Doina Precup. Revisiting heterophily for graph neural networks. In *NIPS*, 2022.
- [Ma *et al.*, 2021] Yao Ma, Xiaorui Liu, Neil Shah, and Jiliang Tang. Is homophily a necessity for graph neural networks? In *ICLR*, 2021.
- [Microsoft, 2021] Microsoft. Neural Network Intelligence, 1 2021.
- [Oono and Suzuki, 2019] Kenta Oono and Taiji Suzuki. Graph neural networks exponentially lose expressive power for node classification. In *ICLR*, 2019.
- [Pei *et al.*, 2019] Hongbin Pei, Bingzhe Wei, Kevin Chen-Chuan Chang, Yu Lei, and Bo Yang. Geom-gcn: Geometric graph convolutional networks. In *ICLR*, 2019.
- [Suresh *et al.*, 2021] Susheel Suresh, Vinith Budde, Jennifer Neville, Pan Li, and Jianzhu Ma. Breaking the limit of graph neural networks by improving the assortativity of graphs with local mixing patterns. In *SIGKDD*, 2021.
- [Veličković *et al.*, 2018] Petar Veličković, Guillem Cucurull, Arantxa Casanova, Adriana Romero, Pietro Lio, and Yoshua Bengio. Graph attention networks. In *ICLR*, 2018.
- [Wang *et al.*, 2022] Tao Wang, Di Jin, Rui Wang, Dongxiao He, and Yuxiao Huang. Powerful graph convolutional networks with adaptive propagation mechanism for homophily and heterophily. In *AAAI*, volume 36, pages 4210–4218, 2022.



- [Wang, 2021] Yangkun Wang. Bag of tricks of semi-supervised classification with graph neural networks. *arXiv preprint arXiv:2103.13355*, 2021.
- [Wu *et al.*, 2019] Felix Wu, Amauri Souza, Tianyi Zhang, Christopher Fifty, Tao Yu, and Kilian Weinberger. Simplifying graph convolutional networks. In *ICLR*, pages 6861–6871. PMLR, 2019.
- [Yang *et al.*, 2019] Liang Yang, Fan Wu, Yingkui Wang, Junhua Gu, and Yuanfang Guo. Masked graph convolutional network. In *IJCAI*, pages 4070–4077, 2019.
- [Yang *et al.*, 2021] Liang Yang, Mengzhe Li, Liyang Liu, Chuan Wang, Xiaochun Cao, Yuanfang Guo, et al. Diverse message passing for attribute with heterophily. In *NIPS*, volume 34, pages 4751–4763, 2021.
- [Zhang *et al.*, 2019] Si Zhang, Hanghang Tong, Jiejun Xu, and Ross Maciejewski. Graph convolutional networks: a comprehensive review. *Computational Social Networks*, 6(1):1–23, 2019.
- [Zhang *et al.*, 2022] Wentao Zhang, Zeang Sheng, Ziqi Yin, Yuezhian Jiang, Yikuan Xia, Jun Gao, Zhi Yang, and Bin Cui. Model degradation hinders deep graph neural networks. In *SIGKDD*, page 2493–2503, New York, NY, USA, 2022. Association for Computing Machinery.
- [Zhu *et al.*, 2020] Jiong Zhu, Yujun Yan, Lingxiao Zhao, Mark Heimann, Leman Akoglu, and Danai Koutra. Beyond homophily in graph neural networks: Current limitations and effective designs. In *NIPS*, volume 33, pages 7793–7804, 2020.
- [Zhu *et al.*, 2021] Jiong Zhu, Ryan A Rossi, Anup Rao, Tung Mai, Nedim Lipka, Nesreen K Ahmed, and Danai Koutra. Graph neural networks with heterophily. In *AAAI*, volume 35, pages 11168–11176, 2021.

## A Dataset Details

For all datasets, we follow GPRGNN [Chien *et al.*, 2021] since it is well open-sourced. All datasets used in the ACM-GCN method [Luan *et al.*, 2022] differed in the number of edges from the same datasets used in the other methods, so we re-run the source code of the ACM-GCN method on the uniform datasets (used by GPRGNN). The results are post on Tab. 1. We also present the results from their paper in the Tab. 8. Exploring minor differences in the datasets is not the focus of this paper.

## B Baseline Details

- **Two-layer MLP** is a neural network without propagation and aggregation rules and only learns node representations from node features.
- **GCN** is a graph convolutional network that aggregates information from the neighborhood on average.
- **GCNII** is a graph neural network using two effective tricks on the basis of GCN: initial residual and identity mapping.
- **BernNet** is a graph neural network that uses Bernstein polynomial approximation to design frequency filters.
- **GPRGNN** adaptively optimizes the Generalized PageRank weights to control the contribution of the propagation process at each layer.
- **ACM** adaptively mixes low-pass, high-pass, and identity channels node-wise before the GCN model to extract more information and address harmful heterophily. As for ACM+ (which uses layer normalization) and ACM++ (which uses residual), we believe that these general tricks do not reflect the ability of the model itself, and the original version of ACM and its variants (ACMII) also have high levels on various datasets, but for the sake of conciseness, we choose ACM as our baseline (the same reason for GCNII rather than GCNII\*).
- **FAGCN** is a frequency adaptive graph neural network, which can adaptively aggregate low-frequency and high-frequency information.
- **GBK** uses homophilous and heterophilous weight matrices to obtain homophilous and heterophilous information, and then adaptively selects the appropriate weight matrix for the node pairs according to the gating mechanism.
- **HOG** utilizes topology and attribute information of graphs to learn homophily degree between node pairs so that it can go beyond the homophily assumption (change the propagation rules under the homophily assumption).
- **WRGAT** promotes assortativity node-wise of graph by building a multi-relational graph on top of the original graph to improve performance (The paper observes that higher assortativity leads to stronger predictive performance).

## C Hyper-parameter Searching Space and Optimal Hyper-parameter Setting

### C.1 Common parameter Searching Space

Table 4 shows the searching space of several common parameters, including learning rate, weight decay, dropout and hidden dimension. We use a Tesla A100 40GB for model training and parameter tuning of all models, considering the modest size of the dataset.

Table 4: The searching space for the common parameters of all methods.

Parameter	Searching space
learning rate	{0.001, 0.002, 0.005, 0.008, 0.01, 0.02, 0.05, 0.08, 0.1}
weight decay	{0, 5e-5, 1e-4, 5e-4, 1e-3, 5e-3}
dropout	{0, 0.1, 0.2, 0.3, 0.4, 0.5, 0.6, 0.7, 0.8, 0.9}
hidden dimension	{64, 128, 256, 512}

### C.2 Specific Parameters for Baselines

We present some specific default parameters for several baseline models. For GPRGNN, we set the order of graph filter (frequency-domain filters often use finite orders) to 10 and the dropout rate before the propagation of GPR weights to 0.5, like BernNet, and let the coefficients  $\gamma_k$  be initialized by PPR and set the  $\alpha$  to 0.5. For FAGCN, the residual coefficient  $\epsilon$  of initial feature is set to 0.3. For WRGAT, the relations of multi-relational computation graph is set to 10. For HOG, all parameter settings follow the authors' settings. For GBK, the hyper-parameter  $\lambda$  to balance two losses is set to 30. And other models follow the default public parameter settings.

### C.3 Parameter for NHGCN and NHGCN-SS

Our method contains both common and specific parameters, shown in Table 4 and Table 5, respectively. *Activation function* will be chosen between ReLU and tanh, as [Luan *et al.*, 2019] highlight the advantage of tanh in maintaining feature differentiation. *Hop* is chosen from  $\{1, 2, 3\}$  because we consider the *NH* of a node as a local metric, and different graphs have different applicability to locality assumption. *Add self-loop* refers to whether the self-loop is added in the GCN-like aggregation, i.e., *Yes* means adopting  $\text{norm}(\mathbf{A}) = (\mathbf{D} + \mathbf{I})^{-1/2}(\mathbf{A} + \mathbf{I})(\mathbf{D} + \mathbf{I})^{-1/2}$  and *No* means adopting  $\text{norm}(\mathbf{A}) = \mathbf{D}^{-1/2}\mathbf{A}\mathbf{D}^{-1/2}$ . *Combiner* will pick from three commonly used ones, including  $\{\text{add}, \text{concatenate}, \text{maxpooling}\}$ , as described in Eq. (10). The threshold  $T$  used to distinguish between high and low *NH* groups is only adjusted as the denominator. For brevity, it is presented as an inverted form  $1/T$  in Table 5.  $1/T$  practically varies from 2 to  $C$ , in 0.1 intervals, as well as two quartiles of .25 and .75. It starts from 2 because  $1/T < 2$  means that one class is in the majority and the neighborhood label distribution has not yet reached the point where it can be measured using *NH* metric. We use open source toolkit NNI [Microsoft, 2021] and its built-in TPE [Bergstra *et al.*, 2011] algorithm to tune the hyper-parameters according to the validation accuracy. The optimal parameters are presented in Tab. 6 and 7.

Table 5: Specific Hyper-parameter Searching Space for NHGCN and NHGCN-SS.

Parameter	Searching space
activation function	{ReLU, tanh}
hop	{1, 2, 3}
add self-loop	{Yes, No}
combiner	{add, concatenate, maxpooling}
$1/T$	{2, 2.1, 2.2, 2.25, 2.3, 2.4, 2.5, 2.6, 2.7, 2.75, 2.8, 2.9, 3, $\dots$ , $C$ }

Table 6: Optimal parameters for NHGCN

	Cora	Citeseer	Pubmed	Photo	Computers	Chameleon	Actor	Squirrel	Texas	Cornell
hidden dimension	512	512	512	512	512	512	512	512	512	64
learning rate	0.1	0.001	0.1	0.05	0.05	0.002	0.1	0.002	0.08	0.01
weight decay	1e-3	0	1e-4	5e-5	5e-5	0	1e-3	0	1e-4	5e-4
dropout (aggregation layer)	0.9	0.7	0.5	0.9	0.4	0	0.7	0.4	0.7	0.6
dropout (combiner)	0.3	0.5	0	0.7	0.4	0.7	0.5	0.6	0.5	0.5
activation function	ReLU	ReLU	ReLU	ReLU	ReLU	tanh	ReLU	tanh	ReLU	ReLU
hop	1	1	1	3	1	2	2	1	1	3
add self-loop	Yes	Yes	Yes	No	No	No	Yes	No	No	No
combiner	maxpooling	maxpooling	add	maxpooling	add	add	add	maxpooling	add	maxpooling
$1/T$	2.25	3.25	3.5	3.75	4	4.1	3.5	4	5	3.8

Table 7: Optimal parameters for NHGCN-SS

	Cora	Citeseer	Pubmed	Photo	Computers	Chameleon	Actor	Squirrel	Texas	Cornell
hidden dimension	256	512	512	128	64	512	512	256	512	64
learning rate	0.05	0.001	0.1	0.08	0.1	0.002	0.1	0.001	0.1	0.01
weight decay	0	0	1e-4	5e-5	5e-5	0	1e-3	5e-5	1e-3	5e-4
dropout (aggregation layer)	0.9	0.6	0.5	0.8	0.6	0	0.8	0	0.5	0.4
dropout (combiner)	0.4	0.3	0.6	0	0.3	0.6	0.9	0.5	0	0.5
activation function	ReLU	ReLU	ReLU	ReLU	ReLU	tanh	ReLU	tanh	ReLU	ReLU
hop	3	3	2	1	3	1	1	1	3	1
add self-loop	Yes	Yes	Yes	No	No	No	Yes	No	Yes	No
combiner	maxpooling	maxpooling	concatenate	add	add	maxpooling	concatenate	add	concatenate	maxpooling
$1/T$	4	3.5	3	3	6	4.25	4.75	4.75	4.8	3.7

## D Full comparison

We compare our results with those provided in the original papers of baselines except for FAGCN. Since no exact values are provided in its original paper, we adopt the experimental results of FAGCN from the ACM. These models in Table 8 have achieved the current SOTA with dataset split of 60% / 20% / 20% for training / validation / testing. The results of these models are relatively close on homophilous datasets and exhibit relatively larger gaps on heterophilous datasets.

Table 8: Results on real-world benchmark datasets reported in the original papers: Mean Test Accuracy (%)  $\pm$  Standard Deviation (%). Boldface letters are used to mark the best results while underlined letters indicate the second best. “DS” means that the dataset split is different from 60% / 20% / 20%. “-” means that the original paper has no experimental results on this dataset.

	<i>Cora</i>	<i>Citeseer</i>	<i>Pubmed</i>	<i>Computers</i>	<i>Photo</i>	<i>Chameleon</i>	<i>Actor</i>	<i>Squirrel</i>	<i>Texas</i>	<i>Cornell</i>
GeomGCN-I-g	86.26	80.64	90.72	-	-	68.00	31.96	46.01	72.51	65.4
GBK	88.69 $\pm$ 0.42	79.18 $\pm$ 0.96	89.11 $\pm$ 0.23	-	-	-	38.97 $\pm$ 0.97	-	81.08 $\pm$ 4.88	74.27 $\pm$ 2.18
GloGNN++	88.33 $\pm$ 1.09	77.22 $\pm$ 1.78	89.24 $\pm$ 0.39	-	-	<u>71.21 <math>\pm</math> 1.84</u>	37.70 $\pm$ 1.40	<u>57.88 <math>\pm</math> 1.76</u>	84.05 $\pm$ 4.90	85.95 $\pm$ 5.10
GCNII*	88.01	77.13	90.3	-	-	62.48	-	-	77.84	76.49
GPRGNN	88.65 $\pm$ 0.28	80.01 $\pm$ 0.28	89.18 $\pm$ 0.15	DS	DS	67.48 $\pm$ 0.40	39.30 $\pm$ 0.27	49.93 $\pm$ 0.53	92.92 $\pm$ 0.61	91.36 $\pm$ 0.70
CPGNN	83.76 $\pm$ 1.81	67.93 $\pm$ 2.86	82.44 $\pm$ 0.58	-	-	67.19 $\pm$ 2.18	-	54.76 $\pm$ 2.01	63.78 $\pm$ 7.67	-
ACMII-GCN+	<b>89.18 <math>\pm</math> 1.11</b>	81.87 $\pm$ 1.38	90.96 $\pm$ 0.62	-	-	<b>75.51 <math>\pm</math> 1.58</b>	41.50 $\pm$ 1.54	<b>69.81 <math>\pm</math> 1.11</b>	<b>95.41 <math>\pm</math> 2.82</b>	<b>93.93 <math>\pm</math> 3.03</b>
BernNet	88.52 $\pm$ 0.95	80.09 $\pm$ 0.79	88.48 $\pm$ 0.41	87.64 $\pm$ 0.44	93.63 $\pm$ 0.35	68.29 $\pm$ 1.58	41.79 $\pm$ 1.01	51.35 $\pm$ 0.73	93.12 $\pm$ 0.65	<u>92.13 <math>\pm</math> 1.64</u>
FAGCN	88.85 $\pm$ 1.36	<b>82.37 <math>\pm</math> 1.46</b>	89.98 $\pm$ 0.54	-	-	49.47 $\pm$ 2.84	31.59 $\pm$ 1.37	42.24 $\pm$ 1.20	88.85 $\pm$ 4.39	88.03 $\pm$ 5.60
NHGCN	<u>89.05 <math>\pm</math> 1.00</u>	81.95 $\pm$ 0.85	<u>91.58 <math>\pm</math> 0.54</u>	<b>90.73 <math>\pm</math> 0.55</b>	<b>95.24 <math>\pm</math> 0.52</b>	69.85 $\pm$ 1.14	<u>42.86 <math>\pm</math> 1.25</u>	51.02 $\pm$ 1.25	93.61 $\pm$ 3.32	90.64 $\pm$ 4.51
NHGCN-SS	88.72 $\pm$ 1.61	82.18 $\pm$ 0.97	<b>91.64 <math>\pm</math> 0.40</b>	90.72 $\pm$ 0.64	95.23 $\pm$ 0.41	68.99 $\pm$ 1.63	<b>42.94 <math>\pm</math> 0.99</b>	49.99 $\pm$ 1.74	<u>93.93 <math>\pm</math> 2.19</u>	91.28 $\pm$ 4.07